Article ID: 1006-8775(2011) 01-0079-08

ANALYTIC STUDY ON POTENTIAL INSTABILITY AND SPIRAL STRUCTURE OF RAIN CLUSTERS

YU Jie (于 杰), ZHANG Ming (张 铭)

(Laboratory for atmospheric circulation and short-term climate prediction, Institute of Meteorology, PLA University of Science and Technology, Nanjing 211101 China)

Abstract: This paper presents a study on potential instability and spiral structure of unstable rain clusters. First, we develop a linearized non-axisymmetrical mathematic model for rain clusters in circular cylindrical coordinates and acquire its analytic solution. Second, we discuss the potential instability of non-axisymmetrical rain clusters. Finally, we conclude that spiral structures can exist in rain clusters. Our analysis indicates that potential instability occurs when humid stratification coefficient is less than zero. Unstable growth rate increases with the increase of the absolute value for humid stratification coefficient. The simpler the vertical structure of perturbation, the thicker the inversion layer; additionally, the smaller the radius of the rain clusters, the larger the unstable growth rate. Simulation results agree well with those from observation and forecast. The spiral structure simulated by our model is similar to a radar echo, suggesting that rain clusters with spiral structures can occur in the atmosphere. In addition, they are generally close to the model solution in this work.

Key words: rain clusters; mathematic model; spiral structure; potential instability

CLC number: P458.1.21.1 **Document code:** A **doi:** 10.3969/j.issn.1006-8775.2011.01.011

1 INTRODUCTION

Rain clusters refer to a meso-β scale system with an area surrounded by an isohyetal line of 10 mm/h over a life cycle of more than 2 hours and on a spatial scale at the 10–100 km range. After having performed numerical simulation of a case of rain clusters and described their spatial structure, Tao et al. pointed out that in upper air, the pressure and wind fields have apparent non-geostrophic characteristics. Along the pressure gradient, there is a strong non-geostrophic outflow. In mid-altitude, rain clusters often manifest as mesoscale-disturbed troughs; that is, air enters from the rear and becomes a mid-layer inflow. In low altitude, rain clusters display mesoscale-cyclonic vortices with a mesoscale-divergent system in the front, from which the air flows out and enters the cluster, and then becomes a lower-layer inflow[1]. Except for small troughs and ridges, mature and stable mesoscale systems are horizontally quasi-one-dimensional or symmetrical, as described by Zeng[2]. Rain clusters are a prime example of such a system.

The evolution of weather systems has been closely connected with the instability of atmospheric waves[3]. Absolute instability occurs if unsaturated air, with a stratification coefficient of less than zero, is unstable; this is almost impossible in free atmosphere. Unsaturated air is statically stable with a stratification coefficient greater than zero, but it is statically unstable for wet saturated air with a coefficient of humid stratification less than zero. This is called the first kind conditional instability or potential instability. Such potential instability occurs when moist air becomes saturated during its ascent, causing condensation and release of latent heat. Based on their study on the mechanisms of a storm that occurred in the eastern Fujian Province in 2002, Zhen et al.[4] reported that the release of potential instability energy could be a possible mechanism in storm development.

Rain clusters can directly produce storms, and hence a study on rain clusters is theoretically important for mesoscale dynamics and has potential implications in storm forecasting. Initially, we developed an axisymmetric numerical model to study rain clusters. Through analysis, we have acquired its solution. We have analyzed its potential instability and got related unstable criteria[6].

Spiral structure is common in the natural world and occurs on the spatial scales from the Milky Galaxy to the rotary water of sinks. In the atmosphere,

Received 2010-01-25; **Revised** 2010-11-09; **Accepted** 2011-01-18
Foundation item: National Natural Science Foundation of China.(40975031; 41005074)
Biography: YU Jie, Ph.D., primarily undertaking research on mesoscale meteorology.
Corresponding author: YU Jie, e-mail: yujieair@126.com

spiral structure occurs as planetary waves, extratropical cyclones, tropical cyclones, and plateau vortices[7-14]. There is increasing interest in studying the spiral structure in the tropical cyclone due to its perfect spiral cloud bands and close link with the development of the tropical cyclone[15-17]. Most rain clusters appear as having round rather than spiral structures, and many might find interest exploring the existence of these structures. The first step towards this goal is to develop a non-axisymmetric rain cluster model, and to test whether the model can support a spiral structure. For that purpose, we have presented in this paper a rain cluster model that is capable of producing spiral structures. We have focused on the analysis of potential instability and spiral structure of the rain cluster. We have also presented radar echo products of 1-h accumulated rainfall from a cloud cluster with spiral structure, which confirms the existence of spiral structures in reality.

2 MATHEMATICAL MODEL AND SOLUTIONS

Rain clusters are generally a system with meso-β scale circulation airflow. Thus, we can safely assume in this model that the geostrophic parameter f is used as a constant. For rain clusters whose life cycles are less than 3 hours, we can even take $f=0$. In other words, we can ignore the effect of earth rotation. By using Boussinesq approximation to filter sound waves and assuming pseudo-adiabatic condition without friction, we used a circular cylindrical coordinates system to build the following equations.

$$\begin{cases} \dfrac{\partial u}{\partial t}+u\dfrac{\partial u}{\partial r}+\dfrac{v}{r}\dfrac{\partial u}{\partial \theta}+w\dfrac{\partial u}{\partial z}-fv-\dfrac{v^2}{r}=-\dfrac{\partial p}{\rho \partial r} \\ \dfrac{\partial v}{\partial t}+u\dfrac{\partial v}{\partial r}+\dfrac{v}{r}\dfrac{\partial v}{\partial \theta}+w\dfrac{\partial v}{\partial z}+fu+\dfrac{uv}{r}=-\dfrac{\partial p}{\rho r\partial \theta} \\ \dfrac{\partial w}{\partial t}+u\dfrac{\partial w}{\partial r}+\dfrac{v}{r}\dfrac{\partial w}{\partial \theta}+w\dfrac{\partial w}{\partial z}=-\dfrac{1}{\rho}\dfrac{\partial p}{\partial z}-g \\ \dfrac{d\vartheta_{se}}{dt}=\dfrac{\partial \vartheta_{se}}{\partial t}+u\dfrac{\partial \vartheta_{se}}{\partial r}+\dfrac{v}{r}\dfrac{\partial \vartheta_{se}}{\partial \theta}+w\dfrac{\partial \vartheta_{se}}{\partial z}=0 \\ \dfrac{\partial ru}{r\partial r}+\dfrac{\partial v}{r\partial \theta}+\dfrac{\partial w}{\partial z}=0 \end{cases} \quad (1)$$

By dividing the thermodynamic variables into a basic field and its deviation, we introduced a pseudo-equivalent potential temperature deviation ϑ'_{se}, density deviation ρ', and pressure deviation p'. Then,

$$\begin{cases} p(r,\theta,z,t)=\overline{p}(z)+p'(r,\theta,z,t) \\ \rho(r,\theta,z,t)=\rho_0+\rho'(r,\theta,z,t) \\ \vartheta_{se}(r,\theta,z,t)=\overline{\vartheta}_{se}(z)+\vartheta'_{se}(r,\theta,z,t) \end{cases}, \quad (2)$$

where ρ_0, $\overline{p}(z)$, and $\overline{\vartheta}_{se}(z)$ are the typical values of density, pressure, and pseudo-equivalent potential temperature, respectively. At the same height, there are $p' \ll \overline{p}$, $\vartheta'_{se} \ll \overline{\vartheta}_{se}$, and $\rho' \ll \rho_0$. Assuming that the deviation is perturbation and the basic field satisfies the original equation and is statically equilibrium along the vertical direction, then

$$\frac{1}{\rho_0}\frac{\partial \overline{p}}{\partial z}=-g. \quad (3)$$

In the equation above, the following approximation was used[18]:

$$\frac{\rho'}{\rho_0}\approx-\frac{\vartheta'_{se}}{\overline{\vartheta}_{se}}\approx-\frac{\vartheta'_{se}}{\vartheta_{se0}} \quad (4)$$

where ϑ_{se0} is the standard value of pseudo-equivalent potential temperature. We assumed that $\Theta'=g\dfrac{\vartheta'_{se}}{\vartheta_{se0}}$, $\overline{\Theta}=g\dfrac{\overline{\vartheta}_{se}}{\vartheta_{se0}}$, and $N^2_{se}(z)=\dfrac{\partial \overline{\Theta}}{\partial z}=\dfrac{g}{\vartheta_{se0}}\dfrac{\partial \overline{\vartheta}_{se}}{\partial z}$. Inasmuch as this work mainly addresses the effect of geopotential instability on rain clusters and for ease of acquiring analytic solutions, the base flow is assumed negligible. With the stratification coefficient N^2_{se} set constant, we can derive u,v,w,p',Θ' equations after linearization (i.e., the perturbation value includes u, v, w, p', and Θ').

$$\frac{\partial u}{\partial t}=-\frac{\partial}{\partial r}\left(\frac{p'}{\rho_0}\right)+fv \quad (5.1)$$

$$\frac{\partial v}{\partial t}=-\frac{\partial}{r\partial \theta}\left(\frac{p'}{\rho_0}\right)-fu \quad (5.2)$$

$$\frac{\partial w}{\partial t}=-\frac{\partial}{\partial z}\left(\frac{p'}{\rho_0}\right)+\Theta' \quad (5.3)$$

$$\frac{\partial \Theta'}{\partial t}+N^2_{se}w=0 \quad (5.4)$$

$$\frac{\partial ru}{r\partial r}+\frac{\partial v}{r\partial \theta}+\frac{\partial w}{\partial z}=0. \quad (5.5)$$

Eqs. (5.1)–(5.5) are the mathematical models used in our rain cluster model. To solve these linear equations, we assumed that there is no topographic effect and set the boundary condition to be

$$z=0,\quad w=0,\quad z=H,\quad w=0, \quad (6)$$

where H is the height of the tropopause or inversion layer. Under these boundary conditions, and to determine a set of equations of amplitude structures in the r direction for variables $u, v, w, p'/\rho_0, \Theta'$, the standard modular can be set as

$$\begin{pmatrix} u \\ v \\ w \\ p'/\rho_0 \\ \Theta' \end{pmatrix} = \begin{pmatrix} U(r)\cos\dfrac{n\pi z}{H} \\ iV(r)\cos\dfrac{n\pi z}{H} \\ W(r)\sin\dfrac{n\pi z}{H} \\ iP(r)\cos\dfrac{n\pi z}{H} \\ i\Theta(r)\sin\dfrac{n\pi z}{H} \end{pmatrix} e^{i(m\theta-\sigma t)} \quad (7)$$

where m is a non-negative integer. The set of equations for amplitude structures in the r direction can then be determined:

$$\frac{dP}{dr} - fV = \sigma U\,, \quad (8.1)$$

$$\frac{m}{r}P - fU = \sigma V\,, \quad (8.2)$$

$$-\frac{n\pi}{H}P - \Theta = \sigma W\,, \quad (8.3)$$

$$\sigma\Theta + N_{se}^2 W = 0\,, \quad (8.4)$$

$$\frac{drU}{rdr} - \frac{mV}{r} + \frac{n\pi}{H}W = 0\,. \quad (8.5)$$

From Eq. (8.4), we can obtain $\Theta = -N_{se}^2 W/\sigma$. This can then be used in Eq. (8.3) to get

$$P = \left(\frac{N_{se}^2}{\sigma} - \sigma\right)\frac{H}{n\pi}W = \chi W \quad (9)$$

where $\chi = \left(\dfrac{N_{se}^2}{\sigma} - \sigma\right)\dfrac{H}{n\pi} = \text{const}$. From Eq. (8.5), we can obtain

$$W = -\left(\frac{drU}{rdr} - \frac{mV}{r}\right)\frac{H}{n\pi} = -\frac{H}{n\pi}D\,,$$

where $D = \left(\dfrac{drU}{rdr} - \dfrac{mV}{r}\right)$ is divergence. Then,

$$\sigma U + fV = \chi\frac{dW}{dr} \quad (10.1)$$

$$fU + \sigma V = m\chi\frac{W}{r} \quad (10.2)$$

$$\frac{drU}{rdr} - \frac{mV}{r} + \frac{n\pi}{H}W = 0 \quad (10.3)$$

From Eqs. (10.1) and (10.2), we can obtain U and V:

$$U = \frac{\chi}{\sigma^2 - f^2}\left(\sigma\frac{dW}{dr} - fm\frac{W}{r}\right) \quad (11.1)$$

$$V = \frac{\chi}{\sigma^2 - f^2}\left(m\sigma\frac{W}{r} - f\frac{dW}{dr}\right) \quad (11.2)$$

By substituting Eqs. (11.1) and (11.2) into Eq. (10.3) to eliminate U and V, we can obtain the following ordinary differential equation on $W(r)$:

$$r^2\frac{d^2W}{dr^2} + r\frac{dW}{dr} + \left(\lambda r^2 - m^2\right)W = 0 \quad (12)$$

where

$$\lambda = \frac{n^2\pi^2}{H^2}\cdot\frac{f^2 - \sigma^2}{\sigma^2 - N_{se}^2}\,. \quad (13)$$

Variable λ is a constant and m is a non-negative integer. Thus, Eq. (12) is a Bessel equation of the non-negative integer order. When $0 \le r < \infty$, the solution W is the first kind of Bessel function J_m. Then, solving Eq. (12) yields

$$W = \tilde{W}\cdot J_m\left(\sqrt{\lambda}\,r\right) = \tilde{W}\cdot J_m\left(\frac{n\pi}{H}\sqrt{\frac{f^2 - \sigma^2}{\sigma^2 - N_{se}^2}}\cdot r\right) \quad (14)$$

where $\lambda > 0$ and the amplitude $\tilde{W}$ can be any real constant.

3 FORM AND CHARACTER OF SOLUTIONS

3.1 *Model description*

By transforming Eq. (14) and setting

$$\hat{r} = \frac{n\pi}{H}\sqrt{\frac{f^2 - \sigma^2}{\sigma^2 - N_{se}^2}}\,r \quad (15)$$

we can obtain

$$W = \tilde{W}\cdot J_m\left(\hat{r}\right). \quad (16)$$

To present the structure of W, an image of $J_m(x)$ is given in Fig. 1, where $m = 0, 1, 2, 3, 4, 5$.

3.2 *Criterion of growth rate of instability*

Before determining σ and obtaining the criterion on growth rates of instability, we need to define the range (r) of the rain cluster. In this study, $0 < r < \tilde{r}$, and $\tilde{r}$ corresponds to the first value (α_m), where $r \neq 0$ and $J_m = 0$ (Table 1 and Fig. 1). We can also take $\tilde{r}$ as the radius of the rain cluster. In the interval $(0, \tilde{r})$, J_m is always greater than zero.

Table 1. Values of α_m

Zero	$J_0(x)$	$J_1(x)$	$J_2(x)$	$J_3(x)$	$J_4(x)$	$J_5(x)$
1	2.4048	3.8317	5.1336	6.3802	7.5883	8.7715
2	5.5201	7.0156	8.4172	9.7610	11.0647	12.3386
3	8.6537	10.1735	11.6198	13.0152	14.3725	15.7002
4	11.7915	13.3237	14.7960	16.2235	17.6160	18.9801
5	14.9309	16.4706	17.9598	19.4094	20.8269	22.2178

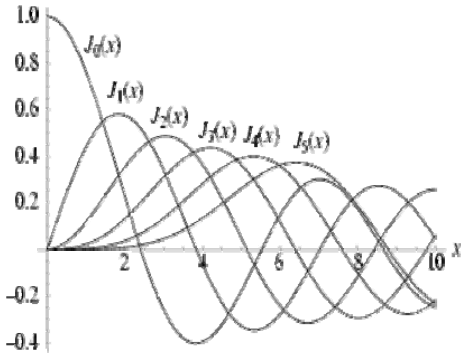

Fig. 1. Bessel function of the first kind

The relationship between $\tilde{r}$ and α_m is determined. From the definition of $\tilde{r}$ and Eq. (14), we can obtain

$$J_m(\alpha_m) = J_m\left(\frac{n\pi}{H}\sqrt{\frac{f^2-\sigma^2}{\sigma^2-N_{se}^2}}\cdot\tilde{r}\right) = 0. \quad (17)$$

Therefore,

$$\tilde{r} = \frac{H}{n\pi}\sqrt{\frac{\sigma^2-N_{se}^2}{f^2-\sigma^2}}\cdot\alpha_m. \quad (18)$$

We can then obtain

$$\lambda = \frac{n^2\pi^2}{H^2}\cdot\frac{f^2-\sigma^2}{\sigma^2-N_{se}^2} = \frac{\alpha_m^2}{\tilde{r}^2} > 0. \quad (19)$$

From Eq. (18), we can obtain a frequency dispersion related to σ^2:

$$\sigma^2 = \frac{(n\pi/H)^2 f^2 + (\alpha_m/\tilde{r})^2 N_{se}^2}{(n\pi/H)^2 + (\alpha_m/\tilde{r})^2}. \quad (20)$$

The right-hand side of Eq. (20) is a real number. Combined with Eq. (7), instability could occur when $\sigma^2 < 0$. Therefore,

$$\frac{(n\pi/H)^2 f^2 + (\alpha_m/\tilde{r})^2 N_{se}^2}{(n\pi/H)^2 + (\alpha_m/\tilde{r})^2} < 0 \quad (21)$$

where σ is a pure imaginary number. In Eq. (21), n, f, $\tilde{r}$, H, and α_m are all greater than 0. If $N_{se}^2 \geq 0$, $\sigma^2 < 0$ cannot be established, and the condition becomes stable. Therefore, for instability to occur, the necessary condition is $N_{se}^2 < 0$. Clearly, the instability is potential instability.

By solving the inequality in Eq. (21), we can obtain the necessary and sufficient conditions of instability as follows:

$$N_{se}^2 < -\frac{n^2\pi^2\tilde{r}^2 f^2}{H^2\alpha_m^2}. \quad (22)$$

From the above inequality, the necessary and sufficient conditions become stricter than the necessary condition of potential instability due to the existence of f. When $f = 0$ (i.e., rain clusters with life cycles of less than 3 h or equatorial rain clusters), the necessary condition is also sufficient. Therefore, f helps stabilize the atmosphere.

3.3 *Effect of environmental coefficients and perturbation structure on the growth rate of instability*

Based on Eq. (20), we can discuss the effect of environmental coefficients and perturbation structure on the growth rate of instability. When $f = 0$,

$$\sigma^2 = \frac{N_{se}^2}{1+\left(\frac{n\pi}{H}\cdot\frac{\tilde{r}}{\alpha_m}\right)^2}, \quad (23)$$

or

$$|\sigma| = \frac{|N_{se}|}{\sqrt{1+\left(\frac{n\pi}{H}\cdot\frac{\tilde{r}}{\alpha_m}\right)^2}}. \quad (24)$$

Clearly, from Eq. (23), $N_{se}^2 < 0$, $\sigma^2 < 0$, and potential instability may occur. Nevertheless, Eq. (24) can also help analyze the effect of environmental coefficients and perturbation structure on the growth rate of instability ($|\sigma|$). The conclusions are as follows:

(1) The more unstable the humid stratification (i.e., $N_{se}^2 < 0$) and the greater $|N_{se}^2|$, the larger the value of $|\sigma|$.

(2) When the atmosphere is potentially unstable, the smaller the value of n (i.e., simpler perturbation

vertical structure), the larger the value of $|\sigma|$. Usually, *n*=1 for rain clusters, and the perturbation is in a vertical semi-wave state.

(3) When the atmosphere is potentially unstable, the larger the value of H (i.e., thicker inversion layer), the larger the value of $|\sigma|$.

(4) When the atmosphere is potentially unstable, the smaller the value of $\tilde{r}$ (i.e., smaller radius of the rain cluster), the larger the value of $|\sigma|$. As a result, most heavy precipitations are locally distributed.

(5) When the atmosphere is potentially unstable, the larger the value of α_m, the larger the value of $|\sigma|$.

Among these conclusions, conclusions (1)−(4) agree well with those from the observation and forecast. In the next paragraphs, we will specifically discuss conclusion (5).

When $f \neq 0$, the situation is complicated. Conclusion (1) can still be established. When $N_{se}^2 < 0$, the smaller the value of f, the larger the value of $|\sigma|$; consequently, f can keep the atmosphere stable. Inasmuch as no direct estimates of the effects of other environmental coefficients on $|\sigma|$ are possible, we carried out a calculation by sampling the following representative values for the environmental coefficients: $N_{se}^2 = -10^{-5}$, $n = 1$, $H = 3$ km, $\tilde{r} = 5$ km, and $\alpha_m = \alpha_2$. When a coefficient changes, whereas others maintain their original values, we can confirm the relationship between $|\sigma|$ and the environmental coefficients. The results indicate that when $f \neq 0$ and with representative environmental coefficients sampled, the above conclusions can still be established (See Figs. 2 & 3).

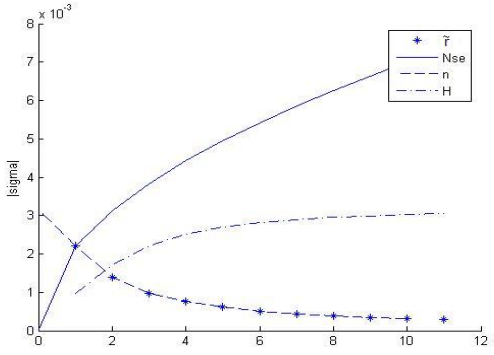

Fig. 2. Variations in growth rate instability $|\sigma|$ with $|N_{se}^2|$, n, H, and $\tilde{r}$. Ordinates: $|\sigma|$, units in $\times 10^{-3}\text{s}^{-1}$; Abscissa: Real line for $|N_{se}^2|$, units in $\times 10^{-5}\text{s}^{-2}$; broken line for n, dash dotted line for *H*, units in km; line with asterisks for $\tilde{r}$, units in 5 km

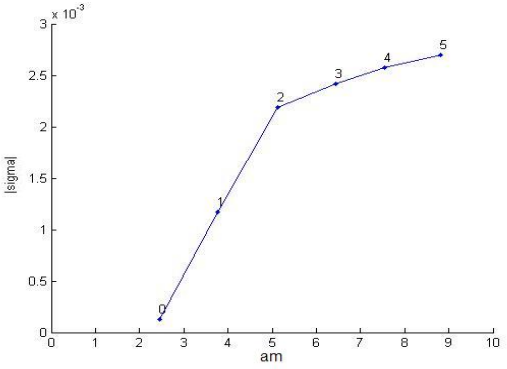

Fig. 3. Variations in growth rate instability $|\sigma|$ with α_m

4 SPIRAL STRUCTURE OF UNSTABLE PERTURBATION

When $m = 0$, the perturbation is independent of θ, and the air motion depends only on r in the horizontal direction. No spiral structure appears in this case (for details, see Tan[6]). We only discussed the case of $m \neq 0$.

By transforming Eq. (14) into Eq. (7) and by considering Eq. (19), we can obtain the spatiotemporal distribution of vertical motion w.

$$w = \mathrm{Re}\left[\tilde{W} \cdot J_m\left(\alpha_m \frac{r}{\tilde{r}}\right) \sin\frac{n\pi z}{H} e^{i(m\theta - \sigma t)}\right]$$

$$= \begin{cases} \tilde{W} \cdot J_m\left(\alpha_m \dfrac{r}{\tilde{r}}\right) \sin\dfrac{n\pi z}{H} \cos(m\theta \pm |\sigma| t) & (25.1) \\ \tilde{W} \cdot J_m\left(\alpha_m \dfrac{r}{\tilde{r}}\right) \sin\dfrac{n\pi z}{H} \cos(m\theta) e^{\pm|\sigma| t} & (25.2) \end{cases}$$

When σ is a real number ($\sigma^2 \geq 0$), w can be expressed by Eq. (25.1); when σ is purely imaginary ($\sigma^2 < 0$), variable w can be expressed by Eq. (25.2). From Eq. (25.2), when air is unstable, the structures of perturbation maintain their original shape and increase only in original position.

To discuss further the horizontal structure of w, we determined the following approximation:

$$J_m\left(\alpha_m \frac{r}{\tilde{r}}\right) \approx \tilde{A} \cdot \sin\left(\frac{\pi r}{\tilde{r}}\right) \qquad (26)$$

where $\tilde{A}$ is maximum amplitude of $J_m\left(\alpha_m \dfrac{r}{\tilde{r}}\right)$ and $r \in [0, \tilde{r}]$ (see Fig. 1 for details). Eq. (26) is the first item of the expanded formula for

$J_m\left(\alpha_m \frac{r}{\tilde{r}}\right)$, with the primary function $\sin\left(\frac{l\pi r}{\tilde{r}}\right)$ ($l = 1, 2, 3, \cdots\cdots$), where $\tilde{A}$ may be other values besides maximum amplitude, as $\tilde{W}$ of Eq. (25) is a random constant. From Eq. (25.2), we can obtain

$$\begin{aligned} &\approx \tilde{W} \cdot \sin\left(\frac{n\pi z}{H}\right) \cdot \sin\left(\frac{\pi r}{\tilde{r}}\right) \cdot \cos(m\theta) e^{|\sigma| t} \\ &= \frac{\tilde{W}}{2} \cdot \sin\left(\frac{n\pi z}{H}\right) \cdot \sin\left(\frac{\pi r}{\tilde{r}} + m\theta\right) e^{|\sigma| t} + \\ &\quad \frac{\tilde{W}}{2} \cdot \sin\left(\frac{n\pi z}{H}\right) \cdot \sin\left(\frac{\pi r}{\tilde{r}} - m\theta\right) e^{|\sigma| t} \\ &= w_1 + w_2 \end{aligned} \tag{27}$$

We can express $\tilde{W} \cdot \tilde{A}$ by using $\tilde{W}$. The solution is the superposition of w_1 and w_2. The difference between w_1 and w_2 is the horizontal structure. The former is $\sin(\pi r / \tilde{r} + m\theta)$ and the latter is $\sin(\pi r / \tilde{r} - m\theta)$. The horizontal structure of w_1 and w_2 are shown in Figs. 4a, 4b, 5a, and 5b, where m =1 or 2, with m representing the numerical measure of spiral structures. In Figs. 4 and 5, both w_1 and w_2 have spiral structures in the opposite direction, indicating that they reflect mutual images of each other. Variables w_1 and w_2 individually satisfy the original equation. The vertical motion of w_1 or w_2 is not zero in the area $r = \tilde{r}$, whereas the vertical motion of the superposition of w_1 and w_2 is zero in the area $r = \tilde{r}$. Two kinds of spiral structures for w_1 and w_2 can also exist in mathematical theory. Physically speaking, however, only w_1 can exist. Since energy only diffuses outward from a finite region, and cannot diffuse inward to a point in order to generate a singular point, it is impossible for w_2 to appear. In the natural world, the spiral structures of eddy galaxies (including the Milky Galaxy) and tropical cyclones in Northern Hemisphere are also in the form of w_1. Hence, the spiral structure of rain clusters is in the form of w_1. Then,

$$w \approx \tilde{W} \cdot \sin\left(\frac{n\pi z}{H}\right) \cdot \sin\left(\frac{\pi r}{\tilde{r}} + m\theta\right) e^{|\sigma| t} = w_1 \tag{28}$$

As for conclusion 5, based on Fig. 1, when $m \neq 0$, then $J_m(0) = 0$, except when $m = 0, J_0(0) = 1$. The obvious difference between the forms of $m = 0$ and $m \neq 0$ is that the former vertical velocity corresponds to the greatest value while the latter is zero. At the same time, the maximum amplitude of the former is bigger than that of the latter. Moreover, the former perturbation is independent of θ and presents circular symmetry, whereas the latter relates to θ and comes with a spiral structure. The larger the value of m, the larger the value of α_m becomes (see Fig. 1 for details). When the atmosphere is potentially unstable, $|\sigma|$ increases with a rise in the number of spiral structure bands m (see Fig. 5 for details). Meanwhile, the larger the value of m, the smaller the amplitude of J_m (see Fig. 1 for details). The two actions constrain each other. We used the linearization model and proper superposition theorem, whose action dominantly depends on the initial field and the life cycle of the perturbation. The cases of $m = 0$ and $m = 1, 2, 3, \cdots\cdots$ are the modes of the solution for the rain cluster model. Therefore, the linear superposition of these modes is also the solution of the model. The superimposition approaches the actual rain clusters much more. Fig. 6 shows the superposition of $m = 0$ and $m = 2$.

In actual observations, the rain clusters often appear as circular symmetries with the peak rainfall at the center. Does the situation from our simulation (i.e., $m \neq 0$) exist in real rain clusters? It is the question we must answer. We studied a rare rainstorm event that occurred in an area in Shanghai in August 25, 2008. From the picture of radar products on one-hour cumulative precipitation (OHP) (Fig. 7), we found a rain cluster with two spiral bands situated near the center of the picture, which corresponds to the northwest of Shanghai. The rainfall at the center of the rain cluster is relatively smaller. As shown in the figure, there are indeed rain clusters with spiral structures similar to the theoretical analysis above, and they are in the form of w_1. The horizontal structure from our model (Fig. 6) is also similar to that of the rain cluster.

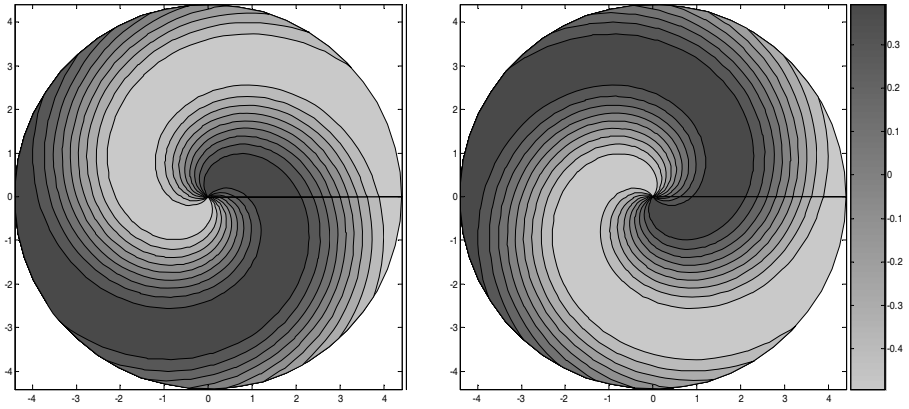

Fig. 4. Horizontal structure of w_1 and w_2 (m=1, $\tilde{W}=1, n=1, z=H/2, t=0$). (a) w_1 and (b) w_2

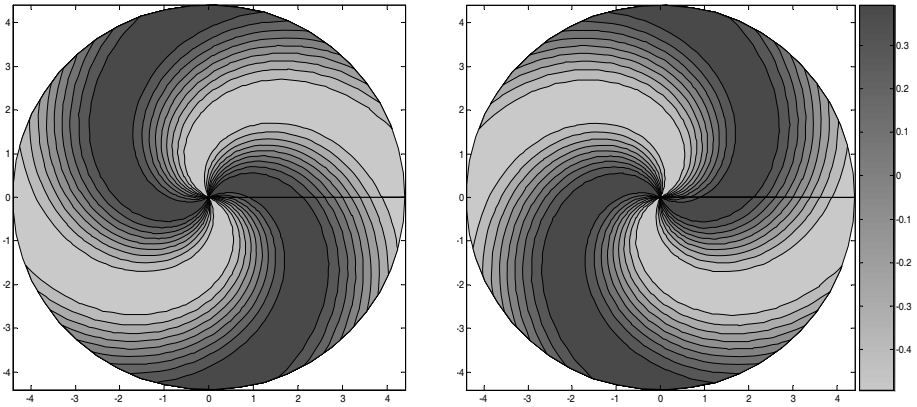

Fig. 5 Horizontal structure of w_1 and w_2 (m=2, $\tilde{W}=1, n=1, z=H/2, t=0$). (a) w_1 and (b) w_2

Lastly, we emphasize that we can follow the same approach to analyze stable cases. For the final solution, we have

$$w=\tilde{W}\cdot J_m\left(\alpha_m\frac{r}{\tilde{r}}\right)\cdot\sin\left(\frac{n\pi z}{H}\right)\cos(m\theta\pm|\sigma|t)$$

$$\approx\tilde{W}\cdot\sin\left(\frac{n\pi z}{H}\right)\cdot\sin\left(\frac{\pi r}{\tilde{r}}+m\theta\pm\sigma t\right). \quad (29)$$

From Eq. (29), the spiral structures are still evident with the vertical motion, but they are different from the case of instability in that spiral bands rotate with time.

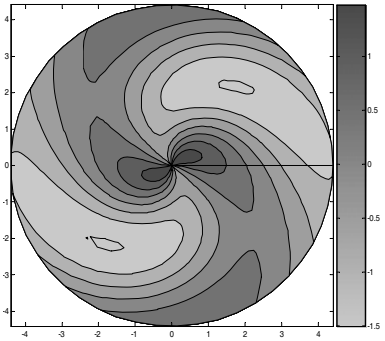

Fig. 6. Horizontal structure of the superposition for $m=0$ and $m=2$. ($m=0$, $\tilde{W}=1$, $m=2$, $\tilde{W}=2$, $n=1, z=H/2, t=0$)

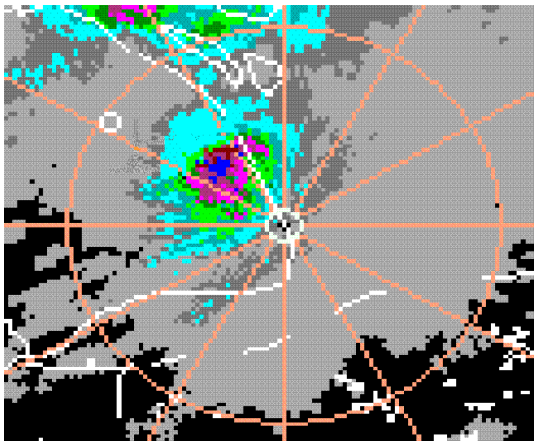

Fig. 7. Radar product chart for 1-h cumulative rainfall at 01:12:22 UTC (August 25, 2008)

5 CONCLUSIONS

In this paper, we discussed the spiral structure and potential instability of rain clusters. First, we developed a linearized non-axisymmetric mathematical model of rain clusters in the circular cylindrical coordinates and acquired its analytic solution. Second, we discussed the potential instability of non-axisymmetric rain clusters. Finally, we concluded that spiral structures could exist in rain clusters. Our analysis indicates that potential

instability occurs when the humid stratification coefficient N_{se}^2 is less than zero, and the instability increases with the increase of the absolute value of N_{se}^2. The simpler the vertical structure of perturbation, the thicker the inversion layer becomes; in addition, the smaller the radius of the rain cluster, the larger the rate of unstable growth $|\sigma|$. Our discoveries conform to the observation and forecast. The spiral structures simulated by our model are consistent with those of the observation and forecast, suggesting that rain clusters with spiral structure can occur in the atmosphere. The spiral structure is also generally the same as that of the model solution in this work. It showed that our rain cluster model is successful. Our analysis also showed that there is a relationship between the spiral bands of a rain cluster and the rate $|\sigma|$ of unstable growth. We found that the linear superposition of solution modes ($m = 0$ and $m \neq 0$) is closer to the observation.

However, our model encountered a few limitations: (1) The assumption that N_{se}^2 is a constant is an oversimplification of reality. (2) The adaptation of linearization in our model, which is a reasonable assumption for the early development stage of a rain cluster, may not be suitable for a mature rain cluster. (3) The effect of the base flow is ignored. In the absence of *f*, the rain cluster can be considered located in an even flow field, without any horizontal or vertical shear. In view of the ability of the current simulation, these limitations are hard to avoid but will be further explored in future studies.

REFERENCES:

[1] WU Qing-li, CHEN Min, WANG Hong-qing, et al. The numerical simulation on meso-βscale flow structure n rain-cluster [J]. Chin. Sci. Bull., 2002, 47(18): 1 437-1 441.

[2] ZENG Qing-cun. The mathematical physics foundation of numerical weather prediction [M]. Beijing: Science Press, 1979: 425.

[3] GAO Shou-ting, SUN Shu-qing. Applying Richardson number to distinguish the instability of mesoscale wave [J]. Chin. J. Atmos. Sci., 1986, 10(2): 171-182.

[4] ZHANG Ming, ZHANG Li-feng, AN Jie. Atmospheric wave spectra analysis and instability, I: The perturbation in two-dimension rotational-stratification [M]. Beijing: China Meteorological Press, 2008: 166pp.

[5] ZHENG Xian-zhao, SHOU Shao-wen, SHEN Xin-yong. Physics parameters analysis of a heavy rainfall event [J]. Meteor. Mon., 2006, 32(1): 102-106.

[6] TAN Yan-yan. A study on potential instability in rain mass-scale [D]. M.S. degree thesis of PLA Univ. of Sci. Eng., 2007, 7-28.

[7] ZHANG Ming, HUANG Si-xun. The non-dispersion solution of nonlinear spiral planetary wave [J]. Acta Meteor. Sinica, 1987, 45(1): 30-38.

[8] ZHANG Ming. Research on instability problem of barotropic vortex [J]. Chin. J. Atmos. Sci., 1995, 19(6): 677-686.

[9] HUANG Hong, ZHANG Ming. Study on destabilization of spiral wave in barotropic vortex [J]. J. Trop. Meteor., 2003, 19(2): 197-202.

[10] LIANG Dan-qing, ZHANG Ming. The spiral wave instability in vortex of two-layer barotropic fluid [J]. J. Trop. Meteor., 2003, 19(4): 405-412.

[11] LIU Xiao-ran, LI Guo-ping. Review and prospect of research on the Tibetan plateau vortex [J]. Arid Meteor., 2006, 24(1): 60-66.

[12] YU Shu-hua. New research advances of the Tibetan Plateau vortex in summer [J]. Torrential Rain Disas., 2008, 27(4): 367-372.

[13] MONTGOMERY M T, ENAGONIO J. Tropical cyclone via convectively forced vortex Rossby-wave in a three-dimensional quasi-geostrophic model [J]. J. Atmos. Sci. , 1998, 55(20): 3 176-3 207.

[14] LUO De-hai. Planetary-scale baroclinic envelope Rossby solitons in a two-layer model and their interaction with synoptic-scale eddies [J]. Dyn. Atmos. Oceans, 2000, 32(1): 27-74.

[15] HUANG Hong, ZHANG Ming. Unstable dynamical properties of spiral bands in tropical cyclones [J]. Acta Meteor. Sinica, 2008. 66(1): 81-89.

[16] MONTGOMERY M T, KALLENBACH R J. A theory of vortex Rossby-wave and its application to spiral bands and intensity changes in hurricanes [J]. Quart. J. Roy. Meteor. Soc., 1997, 123: 435-465.

[17] MOLINARI J. VOLLARO S. Potential vorticity analysis of tropical cyclone intensification [J]. J. Atmos. Sci., 1998, 55(16): 2 632-2 644.

[18] AN Jie. A study about the instability in rainstorm [J]. M.S. degree thesis of PLA Univ. of Sci. Eng., 2004, 13-21.

Citation: YU Jie and ZHANG Ming. Analytic study on potential instability and spiral structure of rain clusters. *J. Trop. Meteor.*, 2011, 17(1): 79-86.